EUROPEAN ORGANIZATION FOR NUCLEAR RESEARCH

CERN-EP/80-54
24 April 1980

A SILICA AEROGEL COUNTER FOR LARGE-ACCEPTANCE HADRON DETECTION

C. Arnault*), P.L. Barberis**), G. Bassompierre***),
W. Burkhardt†), G. Coignet***), U. Dosselli**), P. Heusse*),
F. Montanet††) and M. Schneegans***)

ABSTRACT

Prototype cells of an aerogel Čerenkov counter allowing detection of hadrons outside a large acceptance vertex magnet, are described. The various parameters of the cells are studied and details of their performance are presented. Threshold curves were measured for pions, kaons and protons.

(Submitted to Nuclear Instruments and Methods)

*) LAL, Orsay, France.
**) INFN and Univ. di Torino, Italy.
***) LAPP, Annecy le Vieux, France.
†) Visitor at CERN.
††) Summer Student, CERN, Switzerland.

1. INTRODUCTION

In order to study hadronic final states in deep inelastic muon scattering, it has been decided to complement the European Muon Collaboration Forward Spectrometer[1] with a Vertex Detector System[2]. Good particle identification over a wide acceptance is an essential feature of this additional detector system. For particles produced in the 1-7 GeV/c momentum range, a silica aerogel Čerenkov counter[3] appears to be the only present solution to the problem of filling the momentum gap between the time of flight and the gas Čerenkov techniques.

In the design of the Vertex Detector System, it is planned to use two aerogel counters symmetrically positioned with respect to the beam and covering horizontal angles between 10° and 32°, and vertical angles between -9.50° and +9.50°. They will be located outside the vertex field region, with other detectors placed in front, behind, and also on one side. A Monte Carlo simulation[4] of events generated according to the Feynman and Field model has shown that, to achieve a spatial separation of the outgoing particles in roughly 90% of the cases, each counter has to be divided into about 10 cells. Since the photomultipliers can only be positioned above or below the sensitive volume of the counter, we have to divide it vertically into only two parts, each part being split horizontally into five cells covering 4.4° each. In order to collect as much Čerenkov light as possible, it is necessary to build a well-optimized diffusing box and to accommodate the largest possible number of good quantum efficiency phototubes in the given area.

The final dimensions of the cells (and of the counter), depend on their position relative to the target centre in the whole detector system. Tests were made with two cells, P_1 and P_2, corresponding to two possible locations of the counters with a respective sensitive area of 2 m^2 and 3.2 m^2 each. The aim of the tests was to study the feasibility and the physical characteristics of such counters.

2. TEST SET-UP

The two full-scale prototype cells P_1 and P_2 are shown schematically in fig. 1a and fig. 1b. They use the same wooden structure and have the following properties:

- The active aerogel[5] volume, made of 18 × 18 × 2.7 cm^3 blocks of refractive index n = 1.03, has an area of 80 × 40 cm^2 for P_1 and 65 × 31 cm^2 for P_2.
- The whole internal surface of the box is covered with millipore filter[6]; the back face of the diffusing box is vertical in P_2 but can take a variable orientation in P_1.
- The five 5″ diameter RCA 8854 photomultipliers which were chosen are put as close as possible to each other, taking into account that the iron shielding used is 0.5 cm thick. The photocathodes of the photomultipliers are positioned 10 cm back from their supporting plate in order to improve the shielding against any residual magnetic field. In P_2, the plate supporting the photomultipliers is inclined by ≃ 9° relative to the horizontal plane, as is required by the geometrical acceptance of the vertex detector system.

Test measurements were performed on $\check{C}_A$ (fig. 2) in a 0.3–4.4 GeV/c beam of charged particles at the CERN Proton Synchrotron (PS); the momentum bite was $\Delta p/p \simeq (1\text{-}2)\%$.

Beam particle identification was achieved with the help of three Čerenkov counters:

- $\check{C}_1$ filled with air at atmospheric pressure to flag electrons;
- $\check{C}_2$ filled with CO_2 at 10 kg/cm^2 to detect pions with a momentum larger than 1.5 GeV/c;
- $\check{C}_M$ a silica aerogel counter with refractive index 1.06, used a small part of the time, to sign kaons (protons) with a momentum larger than 1.43 GeV/c (2.70 GeV/c).

The size of the beam-defining scintillation counters A, B, and D was 2 × 2 cm^2 for most of the time, except for fine scans where the B counter was reduced to 0.2 × 2 cm^2.

3. PHOTOMULTIPLIER CALIBRATION AND DETECTOR EFFICIENCY DETERMINATION

3.1 Photomultiplier calibration

To obtain a significant signal, the outputs of four or five photomultipliers have to be added together. As a consequence, all photomultipliers must have the same gain, which means that the one-, two-, and three-photoelectron peaks have to be calibrated to the same ADC channels. This calibration is obtained by the adjustment, with a precision of ±5 V, of the high voltages which vary between 2900 V and 3100 V. A typical photomultiplier pulse height is shown in fig. 3.

We also checked that the HV adjustment can be done with a light-emitting diode (LED) system. Calibration curves relating the HV of each photomultiplier to the distance between peaks, which is proportional to the photomultiplier gain, were obtained after adjustment of the LEDs to a voltage giving pulses similar to the ones obtained with beam particles.

The pulse-height spectra obtained when summing the five photomultiplier outputs are shown in fig. 4 for two cases: 2.2 GeV/c pions in fig. 4a, 3.0 GeV/c kaons in fig. 4b.

3.2 Efficiency determination

The measured quantities are as follows:

- N_b: number of beam-triggering particles;
- N_c: number of beam-triggering particles detected by the aerogel counter; this number depends on the threshold set on the aerogel signal;
- the pulse-height spectrum.

From the two measured numbers, one gets the "measured" efficiency $E_{meas} = N_c/N_b$.

For a mean number of photoelectrons $n_{phe} > 4$ or 5, the number of counts N_0 in the pedestal region is easily determined, and n_{phe} is correctly approximated by $n_{phe} = \log(N_b/N_0)$. For smaller n_{phe}, the extrapolation of the one-photoelectron peak under the pedestal is hazardous and the uncertainty on n_{phe} becomes very large. In that case, we used a method based on the fact that the mean number of photoelectrons is related to the ratio of consecutive peak heights and to the ratio of a minimum value to the preceding maximum value.

The "estimated" efficiency $E_{est} = 1 - \exp(-n_{phe})$ is deduced from these estimates of n_{phe}.

4. MEASUREMENTS AND RESULTS

4.1 Aerogel thickness

Tests were first performed to determine the aerogel thickness to be used when summing the outputs of five photomultipliers. Figure 5 shows the number of photoelectrons obtained when a pion beam hits the centre of the aerogel area. The same behaviour can be observed both for a beam energy below maximum pion detection efficiency (2.2 GeV/c) and for a beam energy at maximum pion detection efficiency (4 GeV/c). The variation of n_{phe} as a function of the aerogel thickness ℓ can be parametrized by the expression

$$n_{phe} \simeq n_{max}(1 - e^{-\ell/\lambda a}) ,$$

with an absorption length $\lambda a = 12 \pm 2$ cm.

We checked that the longitudinal position of the aerogel relative to the photomultipliers was nearly optimized, since switching off any of the five photomultipliers reduced the number of detected photoelectrons by roughly 20%.

Considering the relatively small number of photoelectrons detected, we decided to use 18 cm of aerogel and five photomultipliers.

4.2 Diffusing box

Tests were performed to optimize the diffusing material as well as the shape of the diffusing box.

Using the prototype cell P_1, we found that

- replacing the millipore diffusing layer by aluminized mylar on the face of the box opposite to the photomultipliers produced a 10% reduction in light collection;
- replacing the millipore material by aluminized mylar on both the face opposite to the photomultipliers and the back vertical face caused a reduction of 23%.

We also observed that the addition of a second sheet of the millipore material did not produce any significant improvement; but we measured an increase as big as

25% when adding millipore cones as light-funnels. Furthermore, when the inclination of the back millipore face was changed, the results indicated that the variation of n_{phe} as a function of the beam impact distance (y in fig. 1) to the photomultipliers is steeper when going from a vertical back-face to an inclined back-face. This increase was measured to be 0.14 ± 0.04 photoelectron/10 cm when changing from a vertical to a 25° inclined back-face.

As a result of these measurements we decided to use one layer of millipore membrane as diffusing material with a vertical back-face.

4.3 Effect of incident particle position

It is evident that with the asymmetrical position of the photomultipliers imposed by the final set-up, a variation of the detected n_{phe}, as a function of the distance y to the photomultipliers, has to be expected.

The results of vertical scans performed with 3.4 GeV/c pions are shown in fig. 6. Varying y in the median plane of the cell (x = 0), it can be seen that there is a linear decrease of n_{phe} for both P_1 and P_2, with a slope ≃ 0.02 photoelectrons/cm, except at the end of the cell opposite to the photomultipliers where n_{phe} drops more rapidly. The same effect is observed for a vertical scan performed at x = 12 cm. Figure 7 shows results of horizontal scans done in the central region of P_1 (curve 1), the central region of P_2 (curve 2), and the far end of P_2 (curve 3).

It was also checked with P_2 that an angle of the incident particle with the normal to the entrance plane does not significantly affect the previous measurements, at least for angles smaller than 40°.

From these results and taking into account the small over-all number of photoelectrons, a P_2-type cell was chosen for use in the detector in view of its better efficiency over the whole of its sensitive area.

4.4 Momentum threshold curves

Momentum threshold curves for π, K, and p were obtained with the beam in the centre of the aerogel area.

The pion curve shown in fig. 8 was obtained with the beam triggering condition defined as:

$$A \times B \times D \times \bar{C}_1 \qquad \text{for} \quad p_\pi < 1.5 \text{ GeV/c}$$

and

$$A \times B \times D \times \bar{C}_1 \times C_2 \qquad \text{for} \quad p_\pi > 1.5 \text{ GeV/c} \ .$$

It can be seen that there is a rapid increase of n_{phe} (efficiency) up to 6 photoelectrons (99.7%).

It is more difficult to get the kaon and proton curves, since the condition $A \times B \times D \times \bar{C}_1 \times \bar{C}_2$ is satisfied both by the kaons and by the protons.

Working with a negative beam, the curve shown in fig. 9 was obtained. The number of photoelectrons and the estimated efficiency are deduced from the "peaks-minima" method; a big difference between E_{est} and E_{meas} can be seen. The incorrect value given by $E_{meas} = N_c/N_b$ comes from the overestimate of N_b, which includes antiprotons not detected by $\check{C}_A$ below $\simeq$ 3.6 GeV/c. It can also be seen that, for momenta larger than the $\check{C}_A$ antiproton threshold, E_{meas} is increasing towards E_{est}.

Adding the $\check{C}_M$ requirement in the beam definition, we were able to get a clean kaon signature below $\simeq$ 2.7 GeV/c. We checked that the efficiency then obtained coïncides within errors with the one previously deduced using the "peaks-minima" method.

The proton curve, obtained with a positive beam (small kaon contamination), is shown in fig. 10. There the number of photoelectrons is so small ($\leq$ 1) that even the "peaks-minima" method cannot be used. The measured efficiency gives a low estimate. Owing to the poor counting rate, only a single point of normalization was measured at 4.2 GeV/c by adding the $\check{C}_M$ counter in the beam definition.

The final numbers of photoelectrons for the π, K, and p are shown in fig. 11. Usually, the number of photoelectrons from the Čerenkov effect is given by

$$n_{phe} = A \left[1 - \frac{1}{n^2} \left(1 + \frac{M^2}{p^2} \right) \right] ,$$

where A is a constant characterizing the efficiency in transforming the Čerenkov photons into photoelectrons;

n is the refractive index of the medium;

M is the particle mass;

p is the particle momentum.

Above threshold, each efficiency curve must scale. In Fig. 11, the K and p measured points are compared with the scaling law deduced from the pion measurements; the agreement is very good. From the previous expression of n_{phe}, one can extract the value of n and then the exact momentum threshold value:

$$\Delta n = \frac{1}{2}\frac{M^2}{p^2} \quad \text{at} \quad n_{phe} = 0 \quad \text{if} \quad n = 1 + \Delta n \ .$$

A linear fit to the dependence of n_{phe} as a function of $(M/p)^2$ gives

$$n = 1.031 \pm 0.001 \ ,$$

to be compared with the value, obtained by optical measurement, given by the aerogel manufacturer:

$$n = 1.030 \ ^{+\ 0.003}_{-\ 0.001} \ .$$

The corresponding momentum threshold values are

$$p_\mu = 0.424 \pm 0.009 \text{ GeV/c}$$

$$p_\pi = 0.560 \pm 0.010 \text{ GeV/c}$$

$$p_K = 1.98 \pm 0.03 \text{ GeV/c}$$

$$p_p = 3.76 \pm 0.05 \text{ GeV/c} \ .$$

5. FINAL DESIGN

The previous studies led to the following design for the two detectors symmetrically positioned with respect to the beam, allowing detection over horizontal angles larger than ±9.8°. Each detector that covers an angle of 21.9° in the horizontal plane, consists of 10 P_2-type cells (5 at the top, 5 at the bottom). The upper (lower) frames that support the photomultipliers are inclined by +9° (-9°) with respect to the horizontal plane to keep heavy material out of the acceptance of other detectors.

Each cell, which is tilted relative to the next one by 4.3° in order to reduce traversal of adjacent cells by the same particle, has a 65 cm (high) × 30 cm (wide) × × 18.3 cm (thick) aerogel volume and a 48 cm deep diffusing box. Steel walls, $^{3}/_{10}$ mm thick, separate the cells. The entrance and exit windows are made of aluminium and are $^{2}/_{10}$ mm thick.

All walls of the diffusing box and the front face of the aerogel are covered with millipore; the light collection inside the shielding of the PMs is improved by diffusing cones. Each cell is equipped with five 5″ quantacon photomultipliers RCA 8854.

It is planned to flush nitrogen gas through each cell in order to avoid any deterioration and index changes of the aerogel over a long period.

6. CONCLUSIONS

The studies reported in this paper have allowed the determination of

- the shape and the final dimensions of the counter cells;
- the required aerogel thickness;
- the counter efficiency as a function of both the position and the direction of the incident particle.

We have also measured the counter efficiency as a function of the type and the momentum of the incident particle, using several methods. Threshold curves were then obtained, allowing a good understanding of the detector behaviour.

Acknowledgements

We are indebted to R. Delaruelle, G. Guillhem, G. Juban and J.M. Noppe for their good and efficient mechanical work, and to P. Bernaudin and G. Perrot for their assistance with the electronics. We would like to thank S. Henning for providing us with the aerogel material, J.C. Thompson for the loan of the photomultipliers, A. Muller for the use of his Čerenkov counter, and J. Haas for running the Monte Carlo program. We also acknowledge all the physicists with whom we had stimulating discussions, in particular the members of the European Muon Collaboration.

REFERENCES

1) A large magnetic spectrometer system for high-energy muon physics, European Muon Collaboration, to be published in Nuclear Instruments and Methods.

2) European Muon Collaboration, CERN/SPSC/77-113/p.18/Add.1 (1977) and CERN/SPSC/79-17/p.18/Add.2 (1979).

3) M. Cantin, M. Casse, L. Koch, R. Jouan, P. Mestreau, D. Roussel, F. Bonnin, J. Moutel and S.J. Teichner, Nucl. Instrum. Methods 118 (1974) 177, and J. Chim. Phys. and Phys.-Chim. Biol. 71 (1974) 1537.

J.J. Engelman and M. Cantin, J. Phys., Colloque C3 (1978) C3-57.

M. Benot, P.J. Carlson, S. Tavernier, F. Van Den Bogaert, V.P. Henri, P. Herquet, J. Kesteman, O. Pingot, K.E. Johansson, J. Norrby and J.P. Lagnaux, Nucl. Instrum. Methods 154 (1978) 253.

P.J. Carlson and M. Poulet, Nucl. Instrum. Methods 166 (1979) 425.

S. Henning and L. Svenson, Lund preprint LUNFDG/(NFFL-7001)/1-44/(1979).

4) G. Eszes and E. Nagy, CERN internal note EMC/79/1.

5) Produced by Lund University, Sweden.

6) Produced by Millipore S.A., Mulhouse, France: Ref. HAWP 00010.

Figure captions

Fig. 1 : a) Schematic description of the cell P_1. The detector is viewed by five photomultipliers of the type RCA 8854. The back-face of the diffusing material can take different inclinations.

b) Schematic description of the cell P_2. There is an inside wall which forms a diffusing box reduced in size with respect to P_1. The PM supporting plate is inclined by 9°.

Fig. 2 : Experimental layout. A, B, and D are three beam-defining scintillation counters. $\check{C}_1$ and $\check{C}_2$ are threshold gas Čerenkov counters. $\check{C}_A$ is the studied aerogel counter. $\check{C}_M$ is an aerogel Čerenkov counter used for part of the tests.

Fig. 3 : A typical pulse-height spectrum given by a single PM, in a pion beam of 3.4 GeV/c. The peaks of one and two photoelectrons are clearly visible.

Fig. 4 : A typical pulse-height spectrum obtained by summing the five PM signals:

a) corresponds to a pion beam momentum of 2.2 GeV/c; a mean number of 5.4 ± 0.25 photoelectrons is estimated;

b) corresponds to a kaon beam momentum of 3.0 GeV/c; a mean number of 2.9 ± 0.3 photoelectrons is estimated.

Fig. 5 : Variation of the photoelectron yield with the aerogel thickness for pion beams of 4.0 GeV/c (full circles) and 2.2 GeV/c (crosses) momenta.

Fig. 6 : The yield of photoelectrons as a function of the position of the beam in the y direction (fig. 1).

Curve (1) is for x = 0 in the cell P_2. Corresponding efficiencies are shown with an indication of the error.

Curve (2) is for x = 13 cm in the same cell.

Curve (3) is for x = 0 in the cell P_1.

Fig. 7 : The yield of photoelectrons as a function of the position of the beam in the x direction. The measured points are: (1) at y = 44 cm with cell P_1: (2) at y = +32 cm and (3) at y = 60 cm with cell P_2. A few typical error bars are shown.

Fig. 8 : Pion threshold curve as a function of beam momentum. Open circles are for the estimated number of photoelectrons and corresponding efficiency. Full circles are for the measured number of photoelectrons.

Fig. 9 : Kaon threshold curve as a function of beam momentum. The number of photoelectrons is obtained with the "peaks-minima" method with the corresponding efficiency (full circle). Also shown are the measured efficiencies without $\check{C}_M$ (triangles), which reveal the $\bar{p}$ component of the beam, and with $\check{C}_M$ (open circle).

Fig. 10 : Proton threshold curve as a function of beam momentum. All points are "measured efficiency" values from N_b and N_0 and the deduced number of photoelectrons. For the open circles, $\check{C}_M$ has been added in the trigger.

Fig. 11 : Pion (full circles), kaon (open circles), and proton (triangles) threshold curves. The full curves are deduced from pion measurements. The crosses are measurements obtained with $\check{C}_M$ in the trigger.

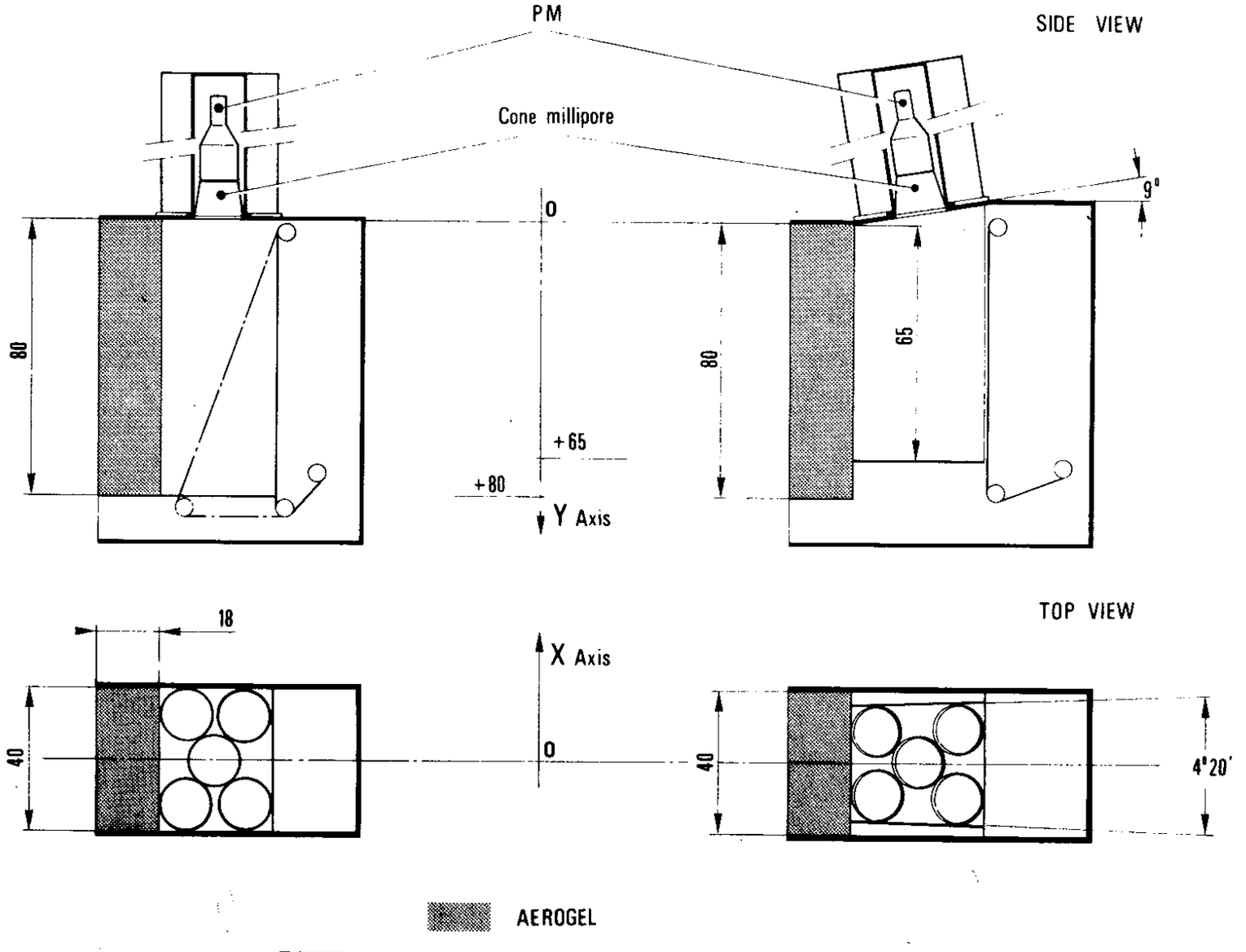
PM
SIDE VIEW
Cone millipore
9°
0
80
80
65
+65
+80
Y Axis
18
X Axis
TOP VIEW
40
0
40
4°20'
AEROGEL
a)
Distances in cm
b)

Fig. 1

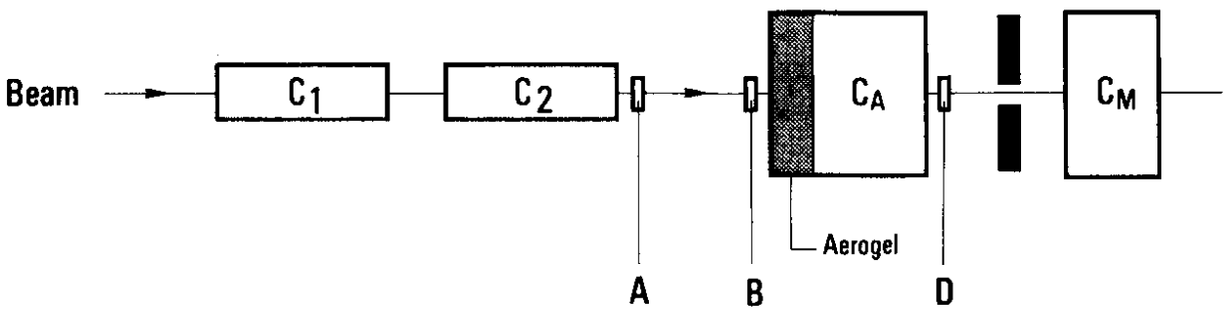

Fig. 2

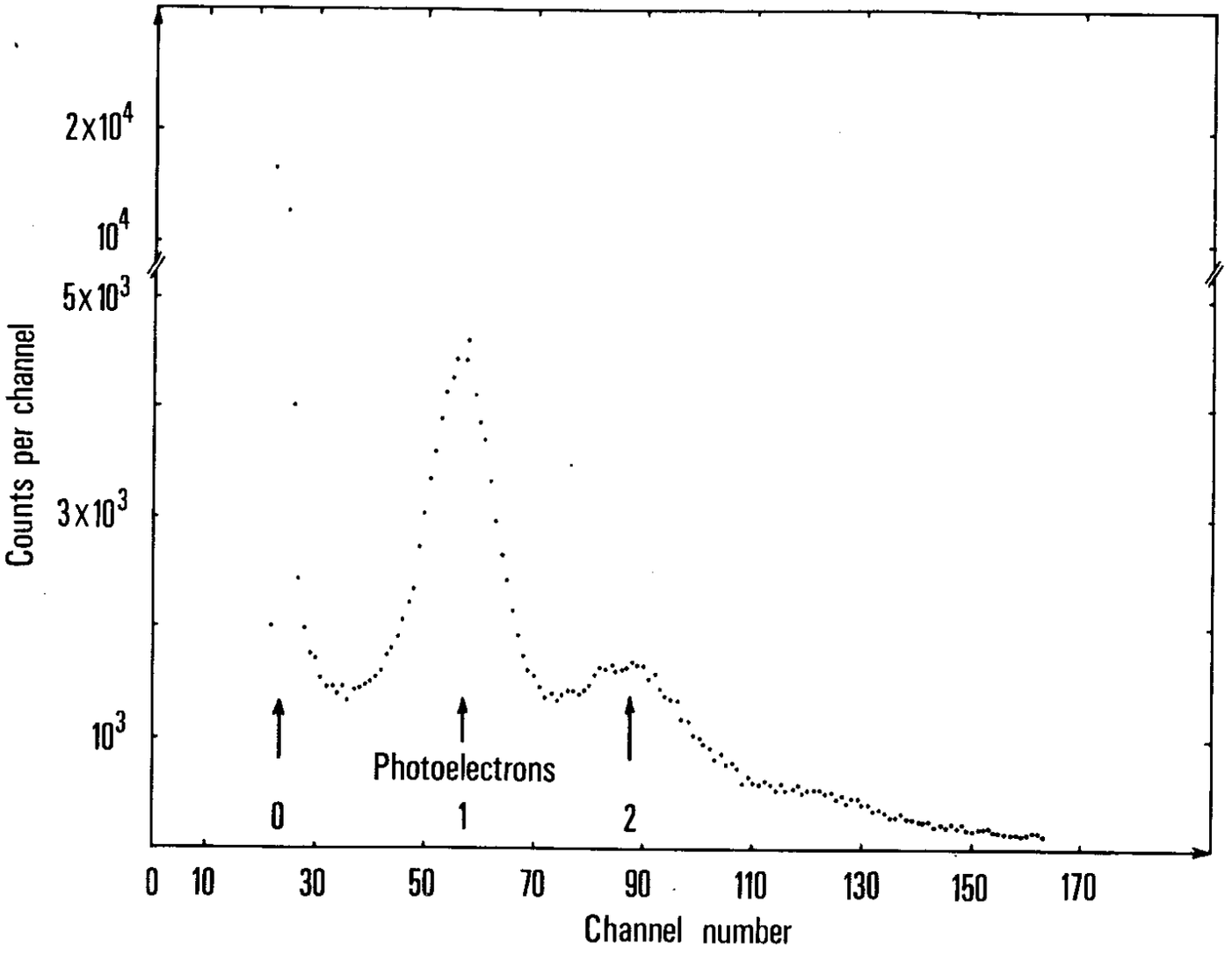
2x10^4
10^4
5x10^3
3x10^3
10^3
Counts per channel
Photoelectrons
0
1
2
0 10 30 50 70 90 110 130 150 170
Channel number

Fig. 3

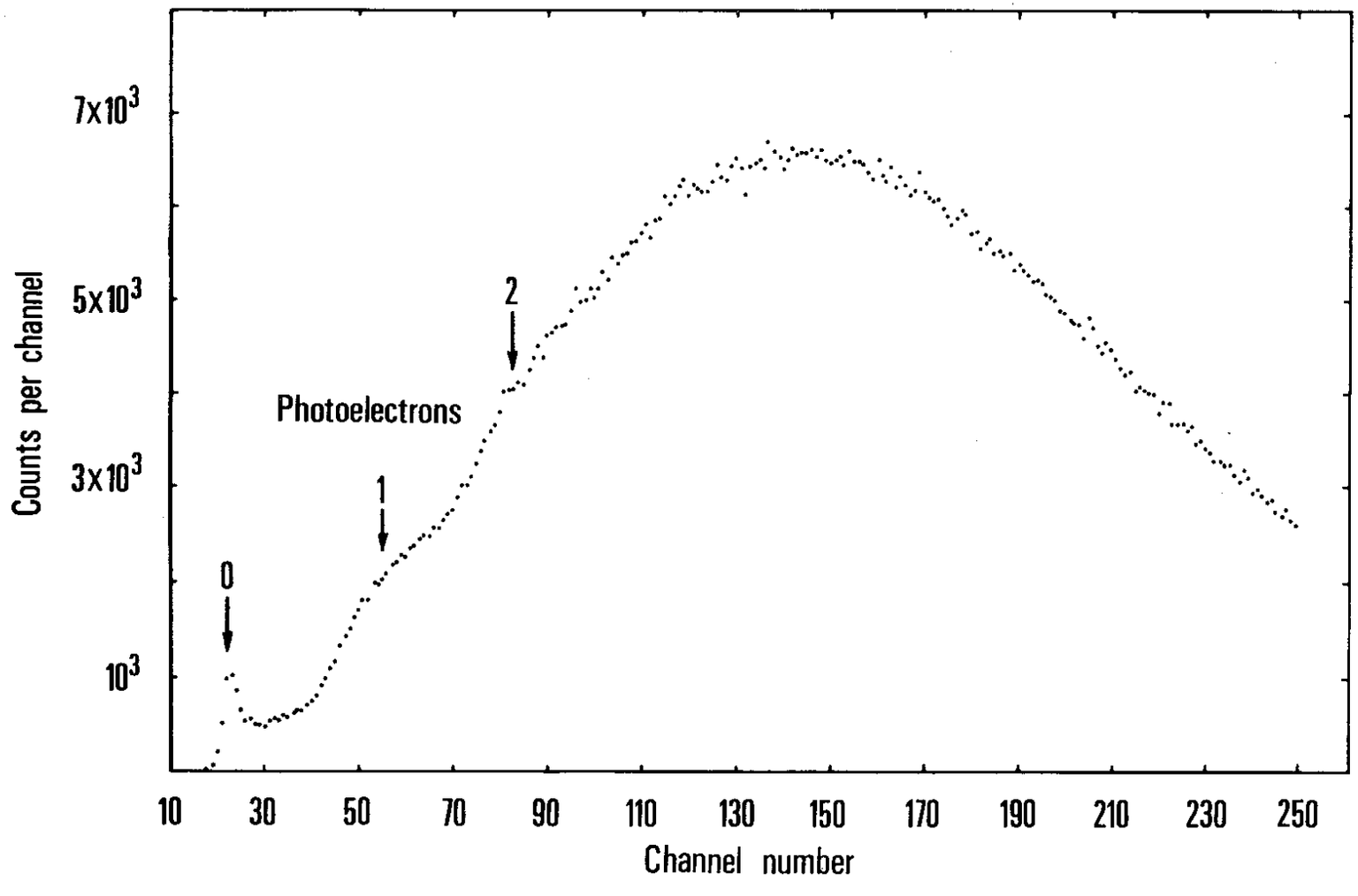
7x10^3
5x10^3
3x10^3
10^3
Counts per channel
Photoelectrons
0
1
2
10
30
50
70
90
110
130
150
170
190
210
230
250
Channel number

Fig. 4a

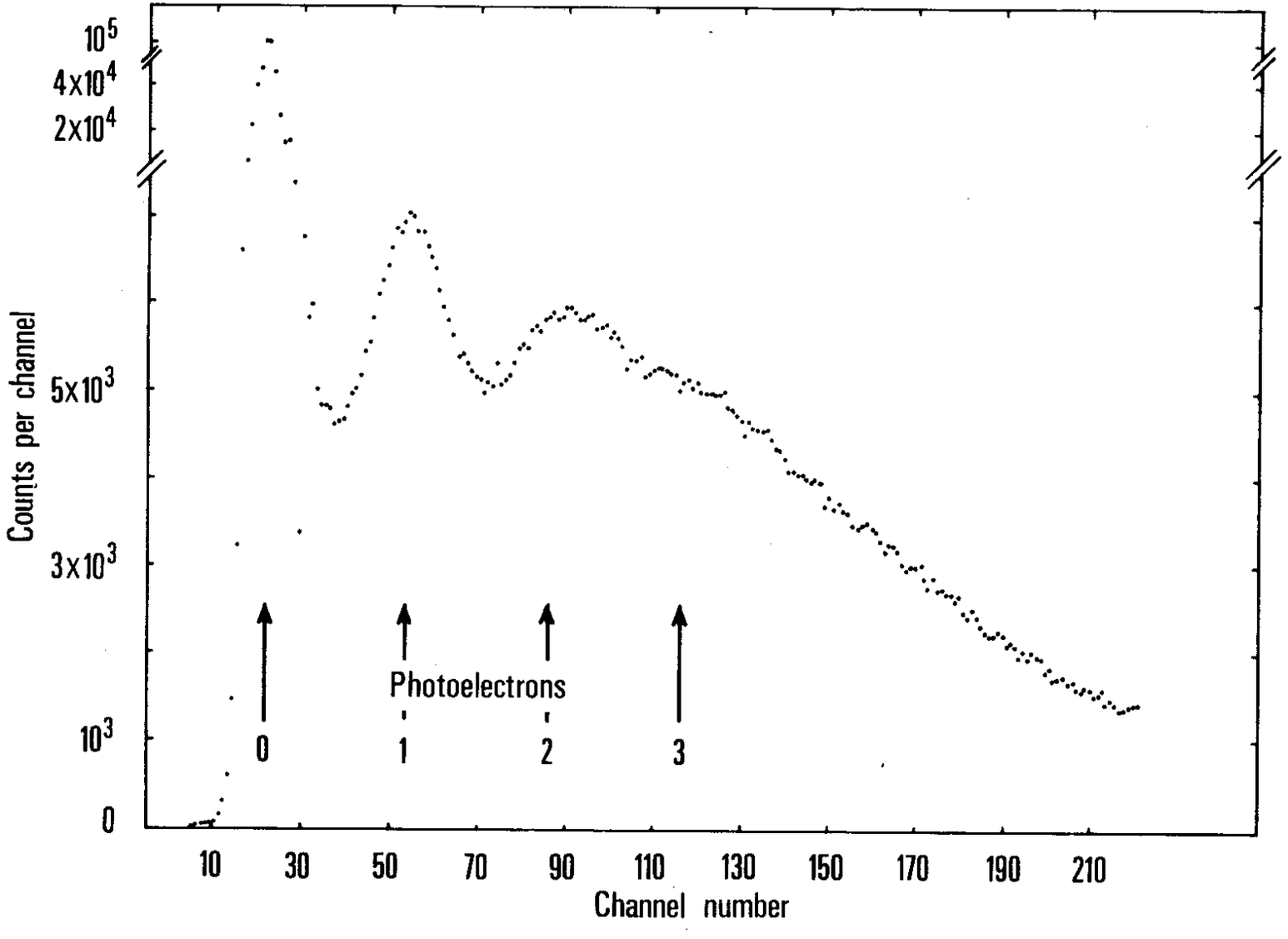
10^5
$4x10^4$
$2x10^4$
$5x10^3$
$3x10^3$
10^3
0
Counts per channel
Photoelectrons
0
1
2
3
10
30
50
70
90
110
130
150
170
190
210
Channel number

Fig. 4b

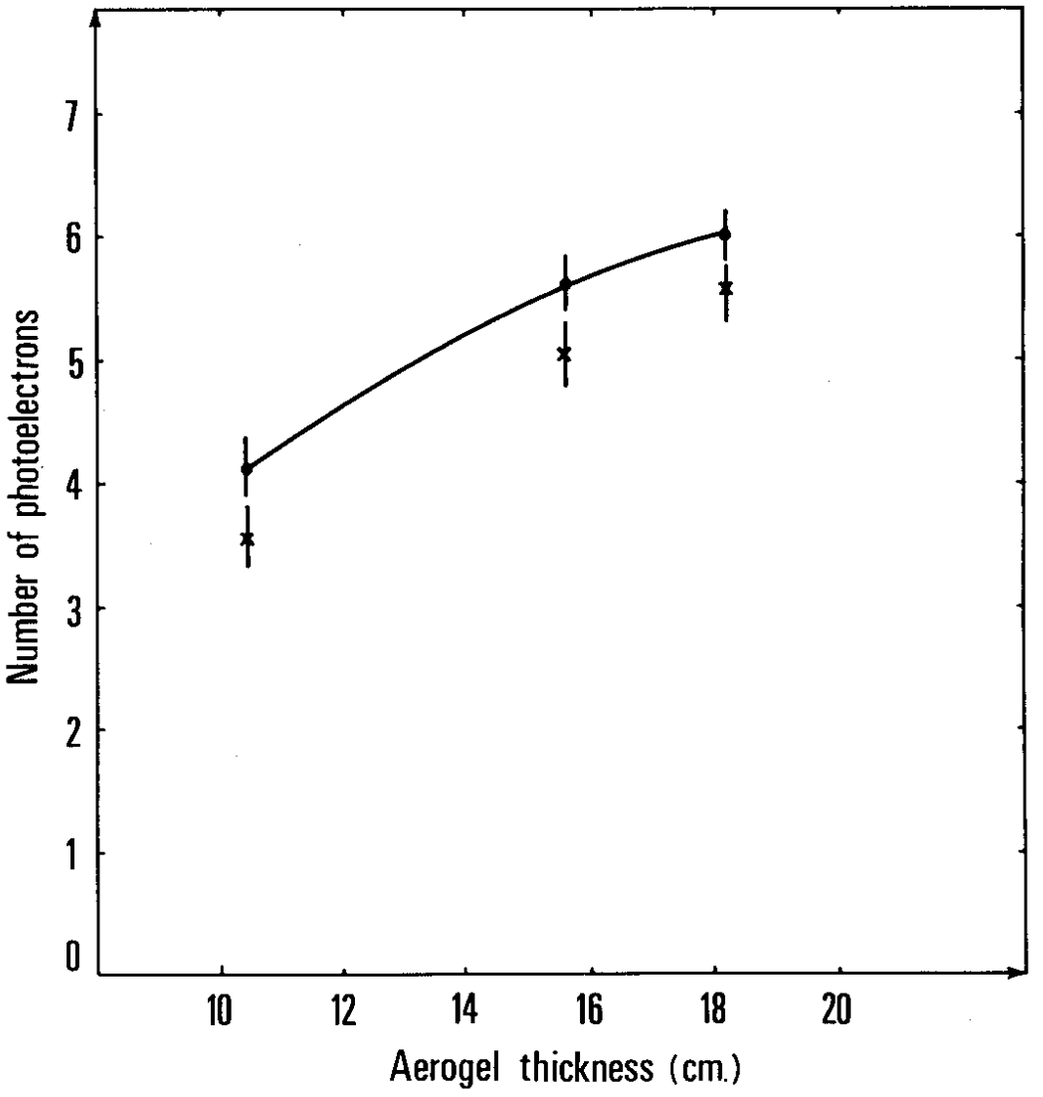
Number of photoelectrons
0
1
2
3
4
5
6
7
10
12
14
16
18
20
Aerogel thickness (cm.)

Fig. 5

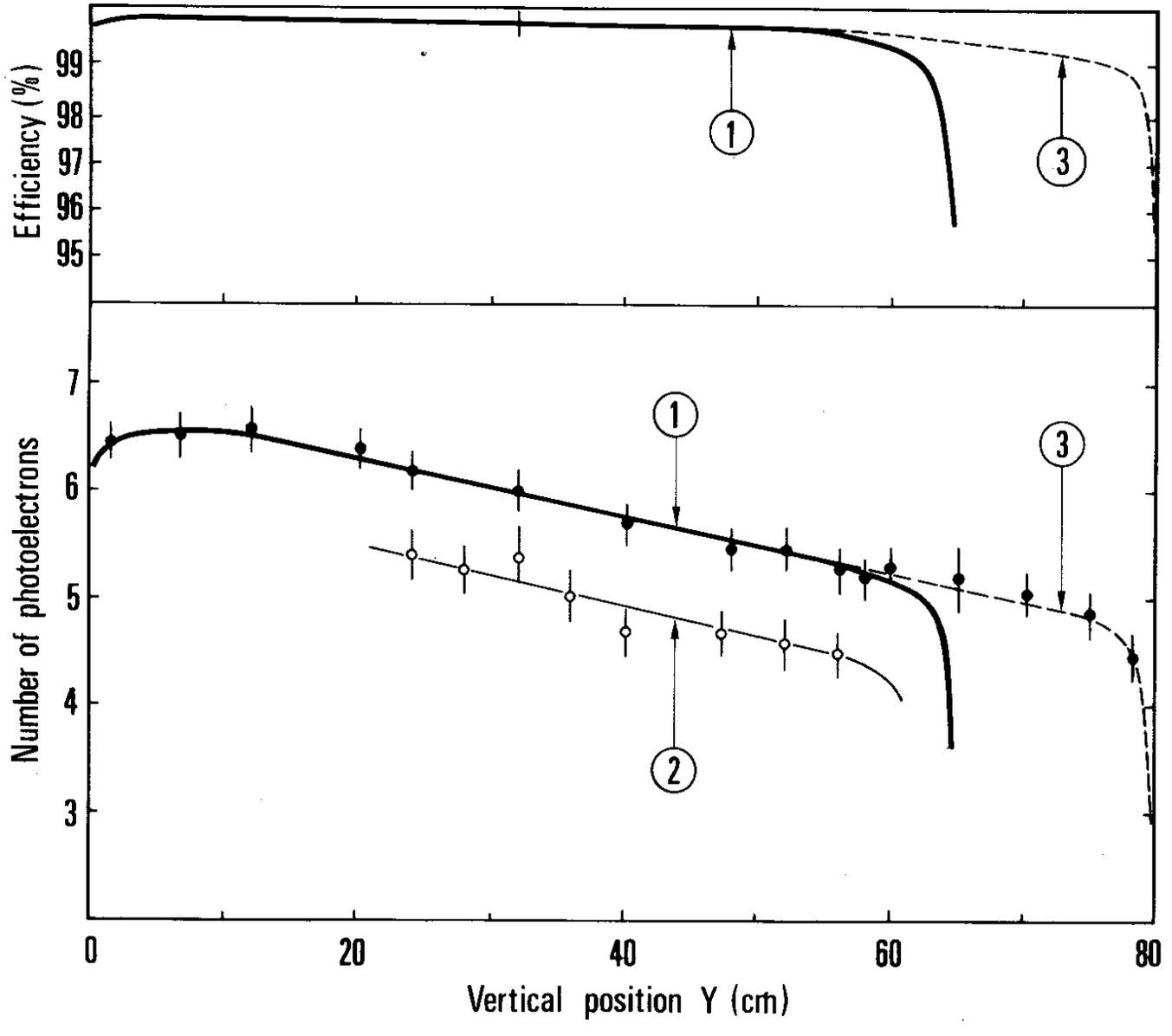
Efficiency (%)
99
98
97
96
95
1
3
Number of photoelectrons
7
6
5
4
3
1
3
2
0
20
40
60
80
Vertical position Y (cm)

Fig. 6

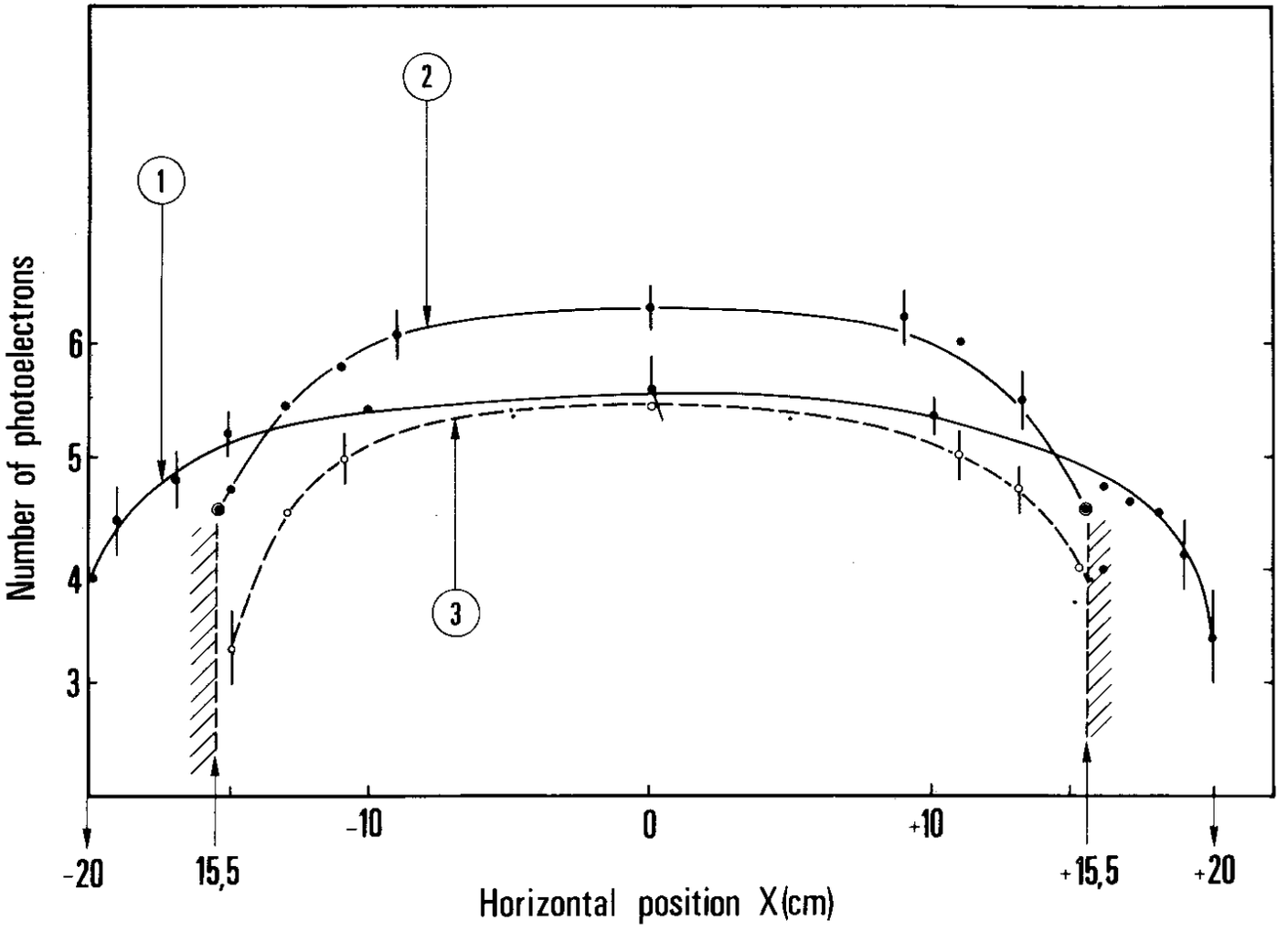
Number of photoelectrons
6
5
4
3
1
2
3
-20
15,5
-10
0
+10
+15,5
+20
Horizontal position X(cm)

Fig. 7

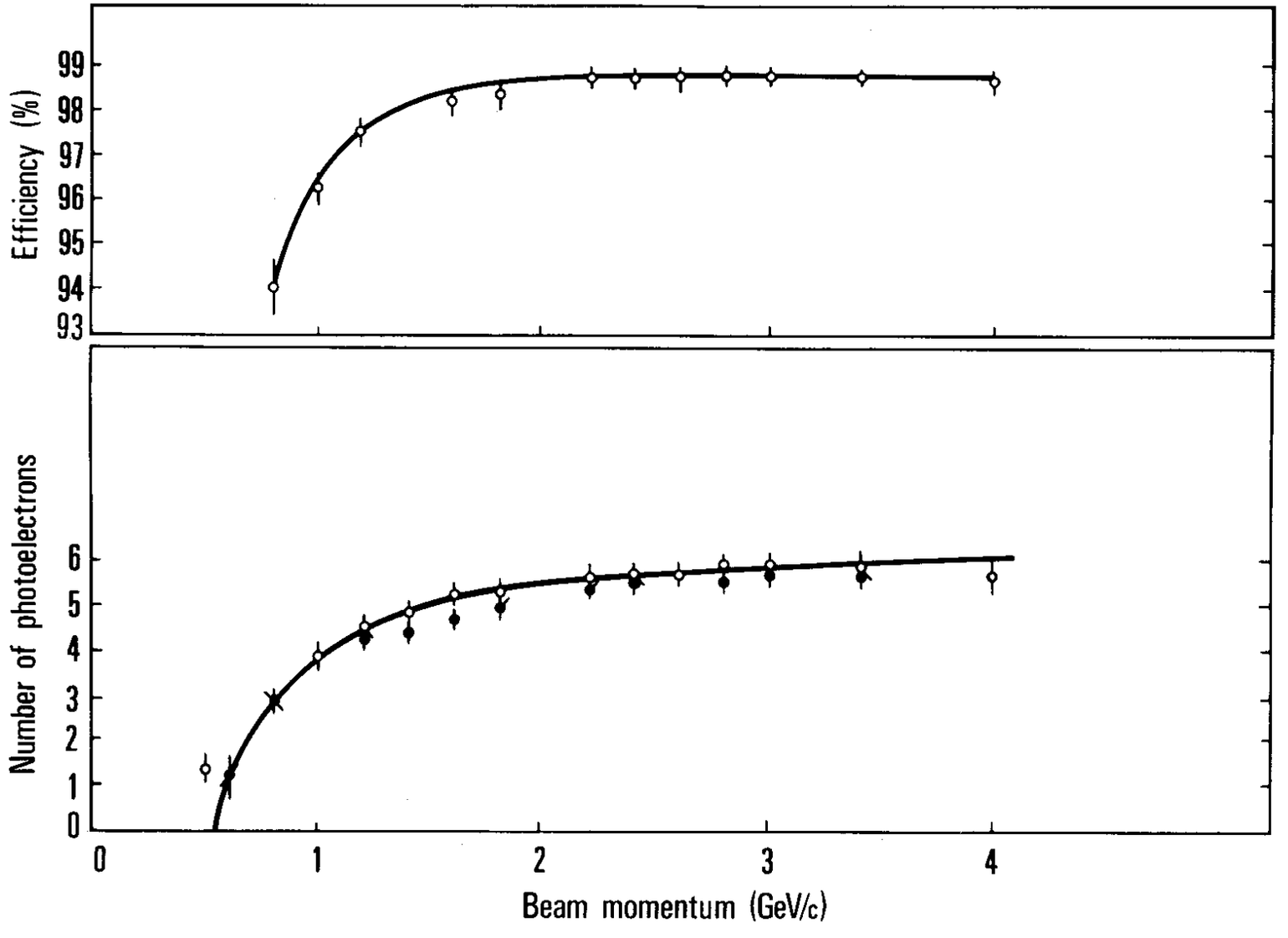
Efficiency (%)
99
98
97
96
95
94
93
Number of photoelectrons
6
5
4
3
2
1
0
0
1
2
3
4
Beam momentum (GeV/c)

Fig. 8

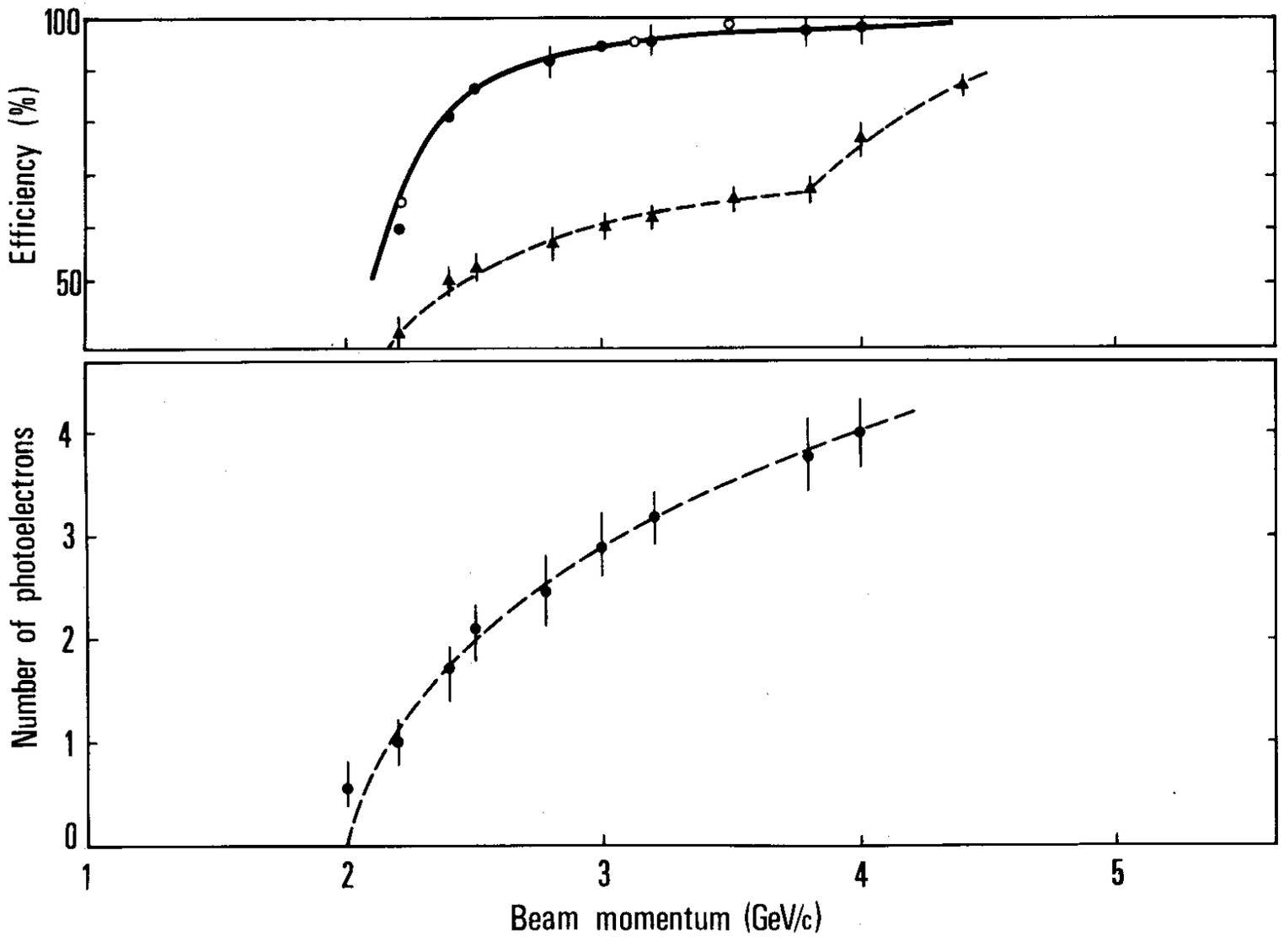
100
50
Efficiency (%)
4
3
2
1
0
Number of photoelectrons
1
2
3
4
5
Beam momentum (GeV/c)

Fig. 9

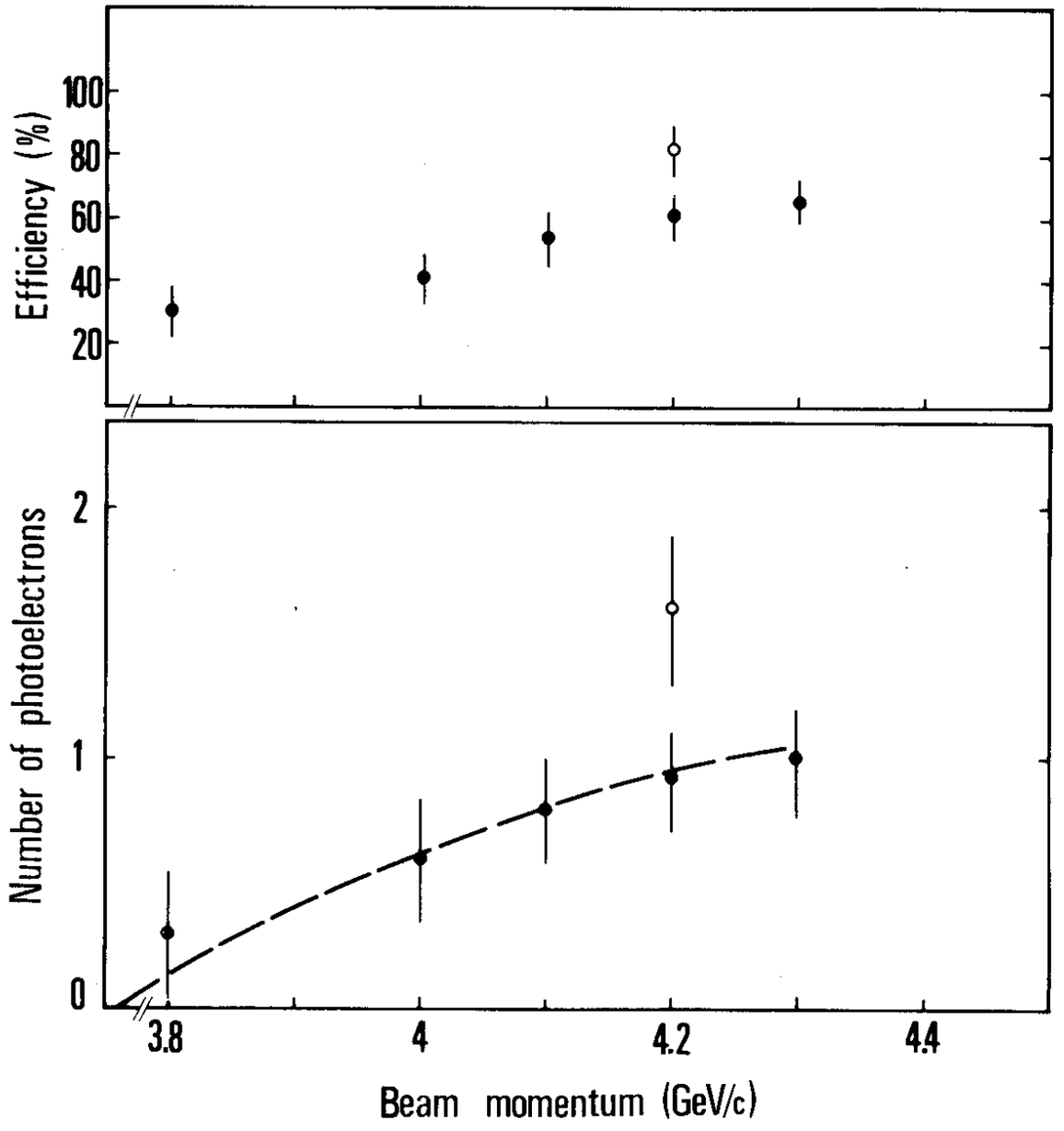
Efficiency (%)
100
80
60
40
20
Number of photoelectrons
2
1
0
3.8
4
4.2
4.4
Beam momentum (GeV/c)

Fig. 10

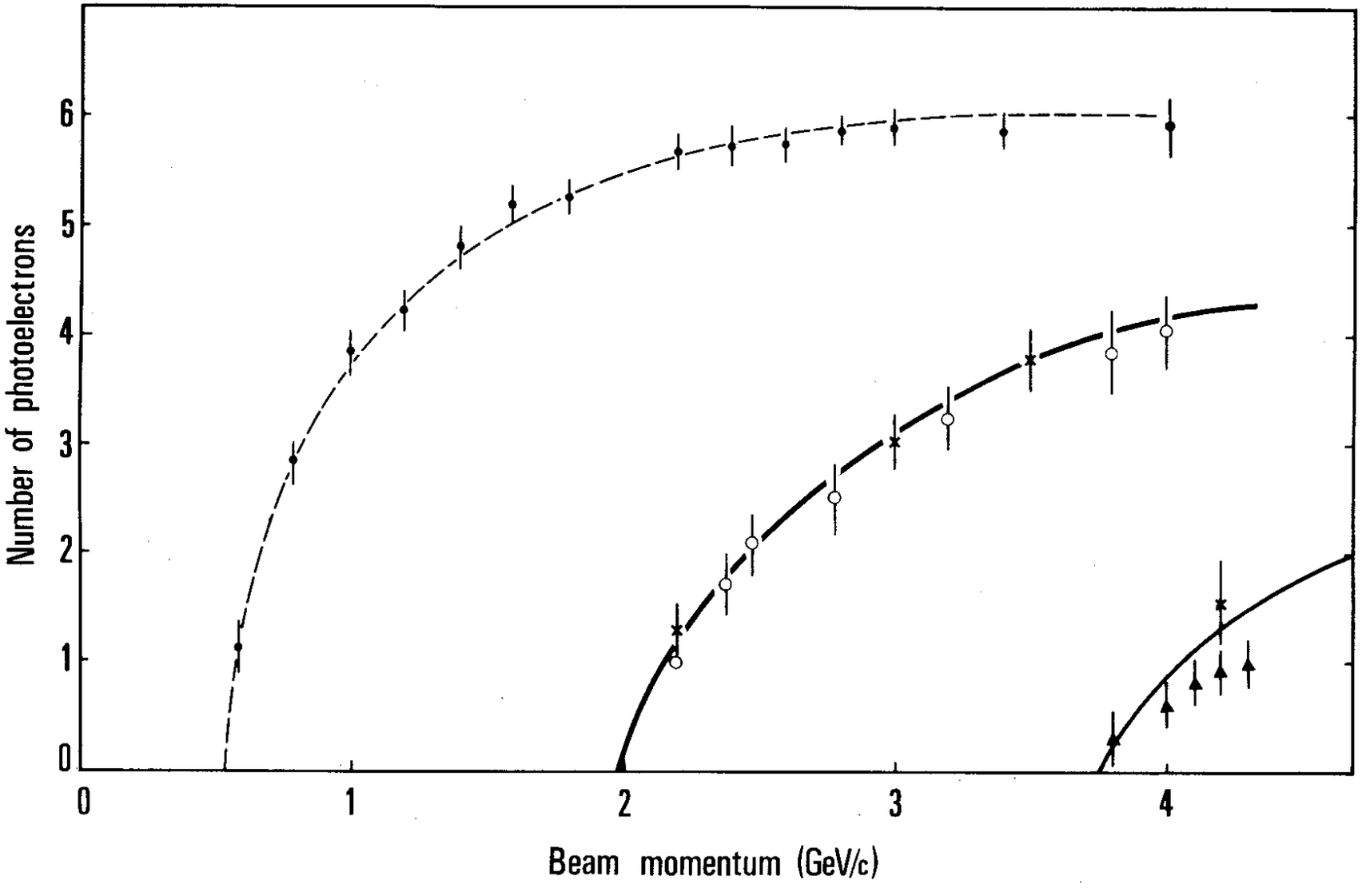
Number of photoelectrons
0
1
2
3
4
5
6
0
1
2
3
4
Beam momentum (GeV/c)

Fig. 11